Supporting Information

Interlayer Engineering of V_2O_5 Anode toward High Rate and Durable Dual Ion Batteries

Wenda Qiu,‡*[a,b], Yunlei Tian,‡[a], Shuting Lin,[a] Aihua Lei,[a] Zhangqi Geng,[a] Kaitao Huang,[a] Jiancong Chen,[a] Fuchun Huang,[a] Huajie Feng*[c] and Xihong Lu*[b]

Guangdong Industry Polytechnic College, Guangzhou 510300, Guangdong, China

[b] *MOE of the Key Laboratory of Bioinorganic and Synthetic Chemistry, KLGHEI of Environment and Energy Chemistry, School of Chemistry, Sun Yat-Sen University, Guangzhou 510275, Guangdong, China*

[c] *Key Laboratory of Electrochemical Energy Storage and Energy Conversion of Hainan Province, Hainan Normal University, Haikou 571158, Hainan, China*

***Corresponding Author.**

E-mail: qiuwd3@mail3.sysu.edu.cn (W.D. Qiu), Fenghuajiehk@163.com (H.J. Feng), luxh6@mail.sysu.edu.cn (X.H. Lu)

‡ These authors contributed equally to this work.

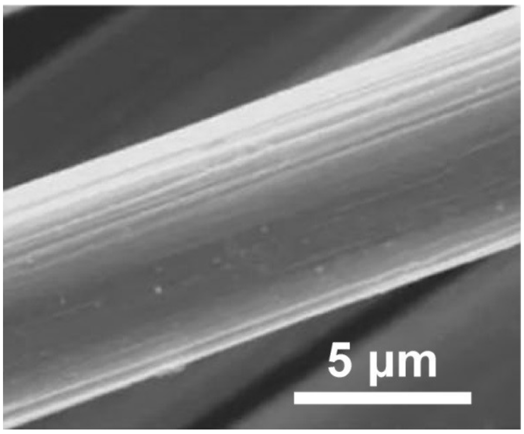

Figure S1. SEM image of carbon fiber cloth

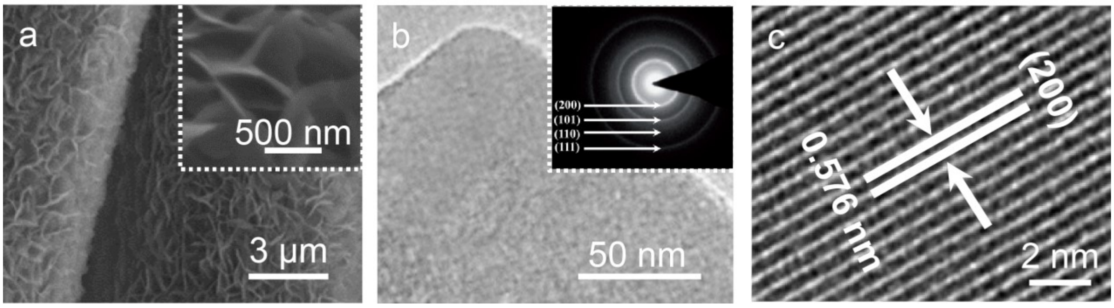

Figure S2. (a) SEM images, (b) TEM images (inset is the SAED pattern), and (c) HRTEM images of α-V_2O_5 NS.

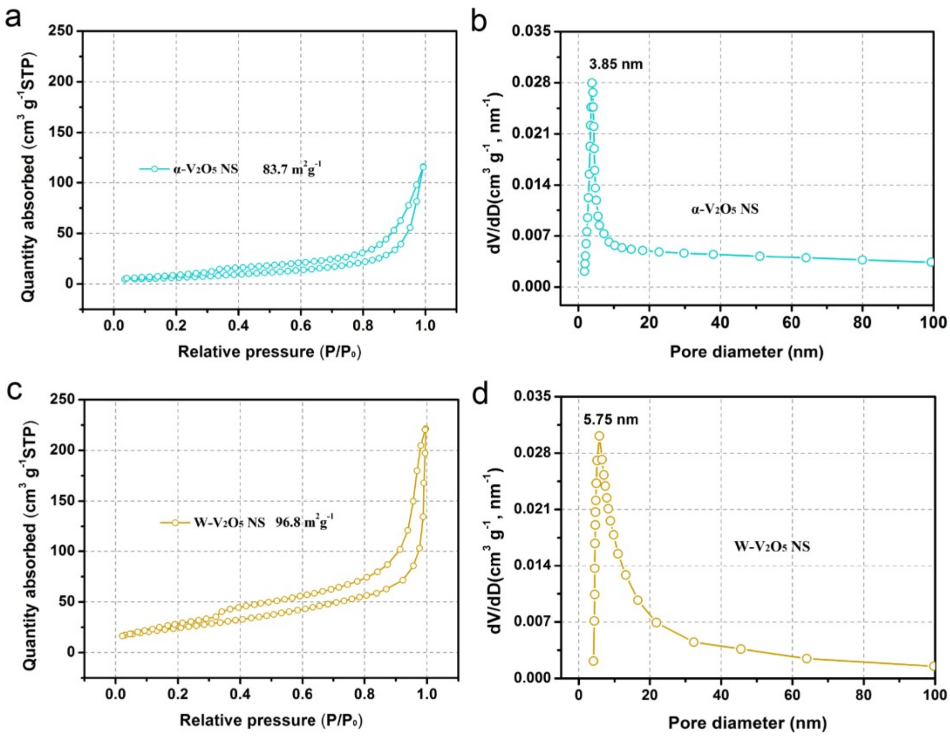

Figure S3. N_2 adsorption-desorption isotherm of (a) α-V_2O_5 and (c) W-V_2O_5 NS. The pore size distribution of (b) α-V_2O_5 and (d) W-V_2O_5 NS.

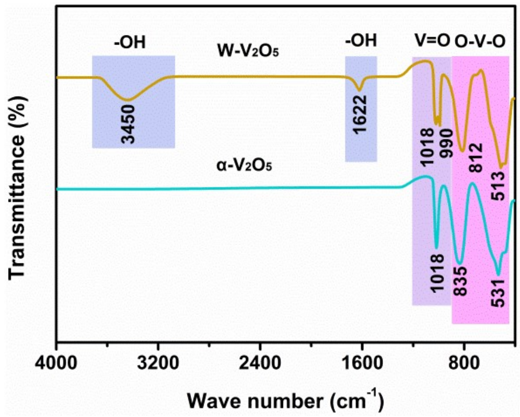

Figure S4. FTIR spectra of α-V_2O_5 and W-V_2O_5 NS.

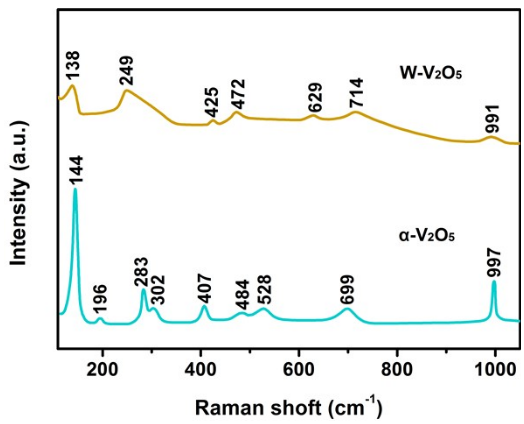

Figure S5. Raman spectra of α-V_2O_5 and W-V_2O_5 NS.

Table S1. Raman peak assignment for α-V_2O_5 and W-V_2O_5 NS.

Vibration modes	Raman shift (cm^{-1})	
	α-V_2O_5 NS	W-V_2O_5 NS
Bending vibrations (B_{1g}, B_{2g} of O–V–O)	144	138
Bending vibrations (A_g, B_{2g} of O–V–O)	196	
Bending vibrations (B_{2g} of V=O)	283	249
Bending vibration (A_g of V–O)	302	
Bending vibrations (A_g of V=O)	407	425, 472
Stretching vibration (A_g of V_3-O)	484	
Stretching vibration (A_g of V_3-O)	528	
Stretching vibration (B_{3g} of V_2-O)	699	629,714
Stretching vibration (A_g of V=O)	997	991

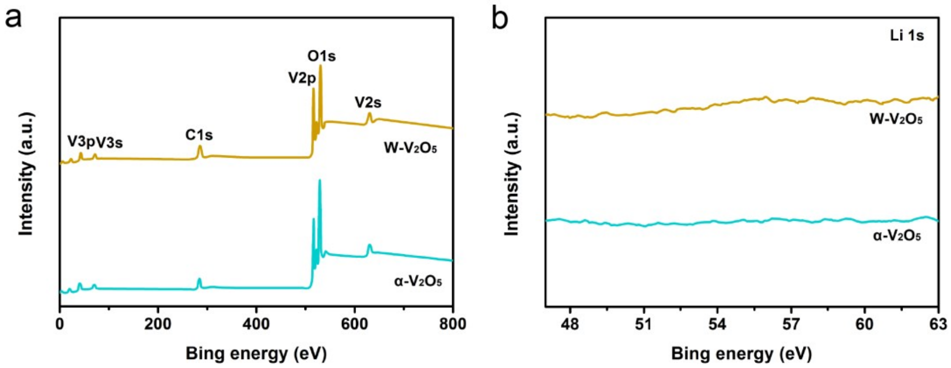

Figure S6. (a) Survey and (b) Li 1s XPS spectra of α-V_2O_5 and W-V_2O_5 NS.

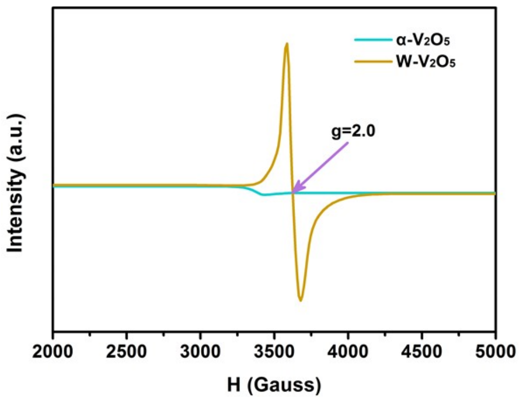

Figure S7. EPR spectra of α-V_2O_5 and W-V_2O_5 NS.

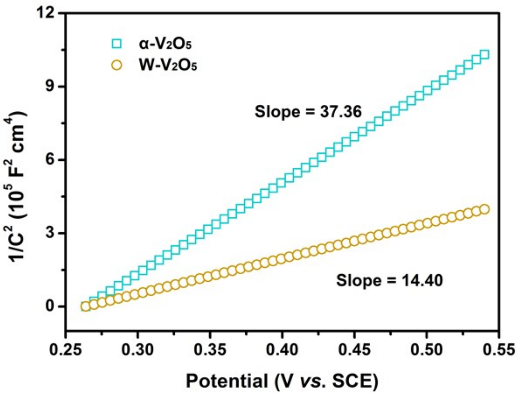

Figure S8. Mott−Schottky plots of α-V_2O_5 and W-V_2O_5 NS.

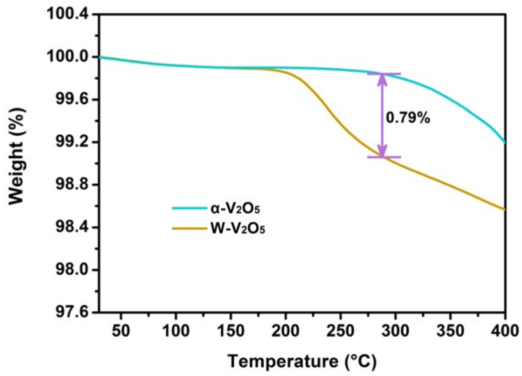

Figure S9. TGA curves of α-V_2O_5 and W-V_2O_5 NS measured in argon atmosphere.

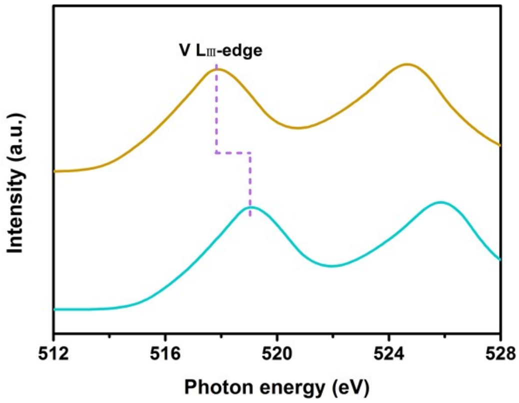

Figure S10. V L edges XANES spectra of α-V_2O_5 and W-V_2O_5 NS.

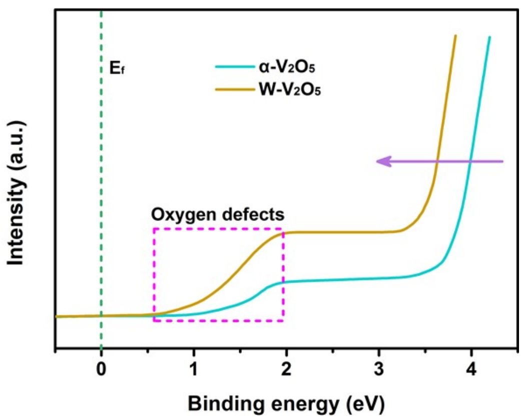

Figure S11. UPS spectra of α-V_2O_5 and W-V_2O_5 NS.

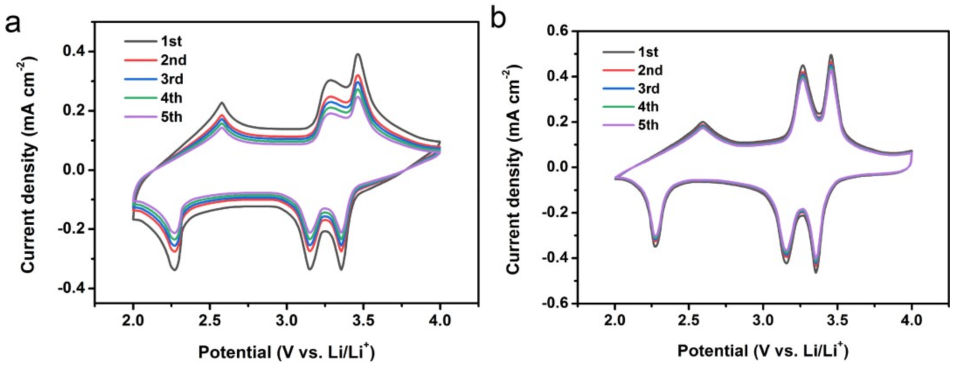

Figure S12. The CV curves at a scan rate of 0.2 mV s^{-1} for the first five cycles of (a) α-V_2O_5 and (b) W-V_2O_5 NS.

Table S2. Comparison of electrochemical performance of W-V_2O_5 NS and the other V_2O_5-based electrodes.

Electrode	Specific capacity	Rate performance	Cycling stability	Ref.
W-V_2O_5 NS	293 mA h g^{-1} at 1 C	47.8% (1 to 40 C)	96.8% after 2000 cycles at 1C	**This work**
$Mn_{0.1}V_2O_5$	265 mA h g^{-1} at 0.1 C	61.9% (0.1 to 20 C)	94% after 500 cycles at 3 C	1
V_2O_5-cG	291 mA h g^{-1} at 0.33 C	56.4% (0.33 to 16.67 C)	94% after 200 cycles at 6.67 C	2
3D-V_2O_5	267 mA h g^{-1} at	51.2% (1 to 20 C)	93% after 50 cycles	3

	0.5 C		at 0.5 C	
3S-V_2O_5 HoMSs/Ni	287.5 mA h g^{-1} at 1.67 C	83% (0.33 to 3.33 C)	92.8% after 200 cycles at 1.67 C	4
V_2O_5/G	291 mA h g^{-1} at 0.1 C	48.7% (1 to 100 C)	92.8% after 600 cycles at 10 C	5
V_2O_5/CNT	242.3 mA h g^{-1} at 0.2 C	27.5% (0.2 to 20 C)	92.3% after 80 cycles at 0.2 C	6
V_2O_5@G	224 mA h g^{-1} at 0.1 C	40.2% (0.1 to 100 C)	91.7% after 200 cycles at 0.5 C	7
V_2O_5	265.9 mA h g^{-1} at 0.1 C	48.9% (0.1 to 2 C)	91% after 100 cycles at 0.33 C	8
Ni–V_2O_5	294 mA h g^{-1} at 0.17 C	56.5% (0.17 to 8 C)	91% after 50 cycles at 1 C	9
V_2O_5/MWCT	292 mA h g^{-1} at 0.1 C	47.3% (0.2 to 4 C)	90% after 100 cycles at 1 C	10
yolk-shelled V_2O_5 microspheres	262 mA h g^{-1} at 0.33 C	65% (0.33 to 8 C)	89% after 50 cycles at 1 C	11
V_2O_5 yolk-shell microsphere	275 mA h g^{-1} at 0.67 C	58% (0.6 to 6.7 C)	87.6% after 50 cycles at 0.17 C	12

V_2O_5 nanoflowers arrays@PRC	281 mA h g^{-1} at 0.2 C	49.8% (0.2 to 10 C)	87.5% after 500 cycles at 2 C	13
multilayer V_2O_5 hollow sphere arrays	293 mA h g^{-1} at 0.5 C	51.9% (0.5 to 20 C)	87.4% after 300 cycles at 5 C	14
V_2O_5 nanobelts	281 mA h g^{-1} at 0.2 C	33.2% (0.5 to 20 C)	86% after 50 cycles at 0.2 C	15
V_2O_5@GCNFs	293 mA h g^{-1} at 0.1 C	36.2% (0.1 to 20 C)	85.7% after 700 cycles at 5 C	16
V_2O_5 nanosheets	275 mA h g^{-1} at 0.2 C	76% (0.2 to 2 C)	82.4% after 250 cycles at 0.33 C	17
rGO/V_2O_5	249 mA h g^{-1} at 0.33 C	45.4% (0.33 to 5 C)	81.5% after 200 cycles at 5 C	18
H-V_2O_5 nanosheets	259 mA h g^{-1} at 0.33 C	54.8% (0.33 to 6.67 C)	81% after 200 cycles at 0.33 C	19
Interconnected V_2O_5 microspheres	278 mA h g^{-1} at 0.5 C	59.7% (0.5 to 10 C)	81% after 200 cycles at 1 C	20
HP- V_2O_5	283 mA h g^{-1} at 0.33 C	42% (0.33 to 6.67 C)	80.2% after 200 cycles at 3.33 C	21

SANs V_2O_5	235.5 mA h g^{-1} at 1 C	26.6% (0.1 to 10 C)	78.6% after 300 cycles at 2 C	22
V_2O_5 microsphere	210.5 mA h g^{-1} at 0.33 C	44.6% (0.33 to 3.33 C)	76.2% after 150 cycles at 1 C	23
V_2O_5-II	285 mA h g^{-1} at 0.33 C	55.3% (0.33 to 10 C)	75.8% after 100 cycles at 1 C	24
V_2O_5/N-graphene	273 mA h g^{-1} at 0.33 C	66.3% (0.33 to 3.33 C)	75.1% after 100 cycles at 0.33 C	24
Sisal-like V_2O_5	261 mA h g^{-1} at 0.2 C	35.4% (0.1 to 10 C)	74.8% after 400 cycles at 1 C	25
V_2O_5 hollow microsphere	250 mA h g^{-1} at 1 C	56% (1 to 10 C)	68.8% after 100 cycles at 1 C	26
V_2O_5 NAs/CC	268 mA h g^{-1} at 0.33 C	46.5% (0.33 to 15 C)	67% after 100 cycles at 2 C	27
V_2O_5/MWNT/PAN	285 mA h g^{-1} at 1 C	46.3% (1 to 20 C)	66% after 100 cycles at 1 C	28

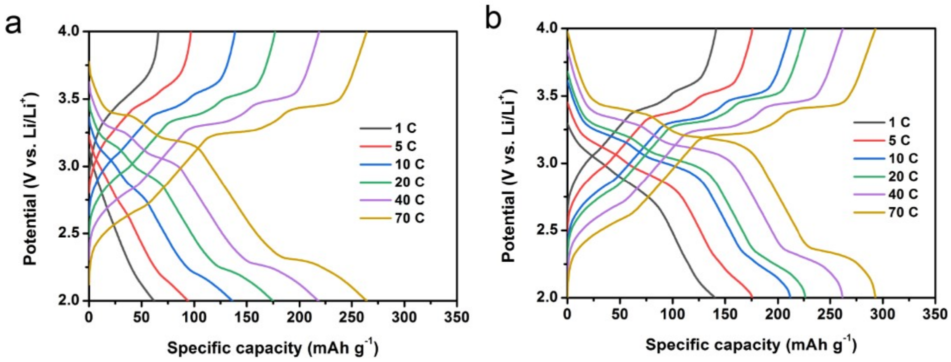

Figure S13. The charge and discharge profiles at different current densities for (a) α-V_2O_5 and (b) W-V_2O_5 NS electrodes.

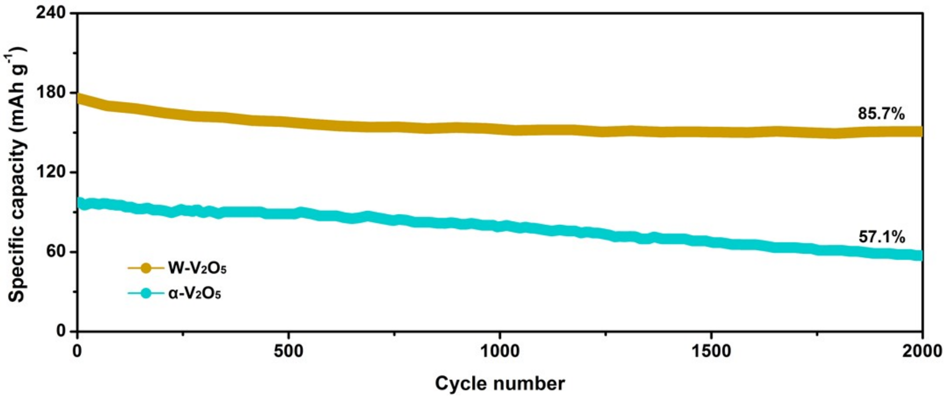

Figure S14. Cycling performance of α-V_2O_5 and W-V_2O_5 NS at high current density of 40 C.

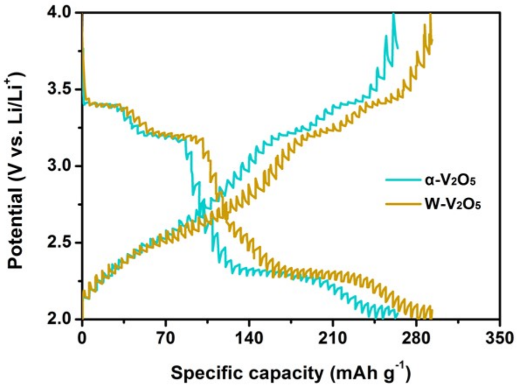

Figure S15. GITT charge discharge curves of α-V_2O_5 and W-V_2O_5 NS electrodes at 1 C.

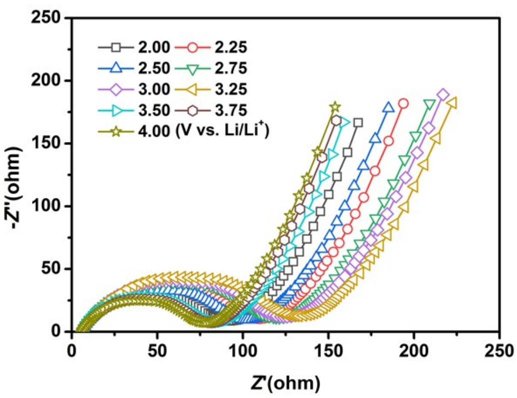

Figure S16. Nyquist plots of α-V_2O_5 NS electrode at different potentials.

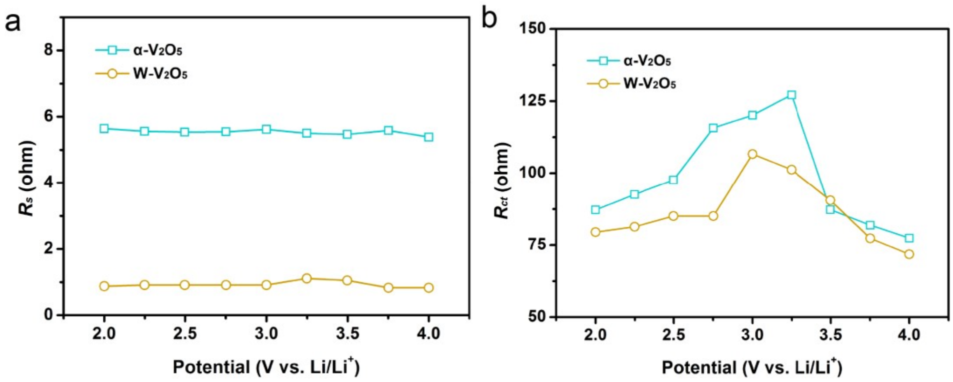

Figure S17. (a) R_s and (b) R_{ct} of α-V_2O_5 and W-V_2O_5 NS electrodes as a function of potential.

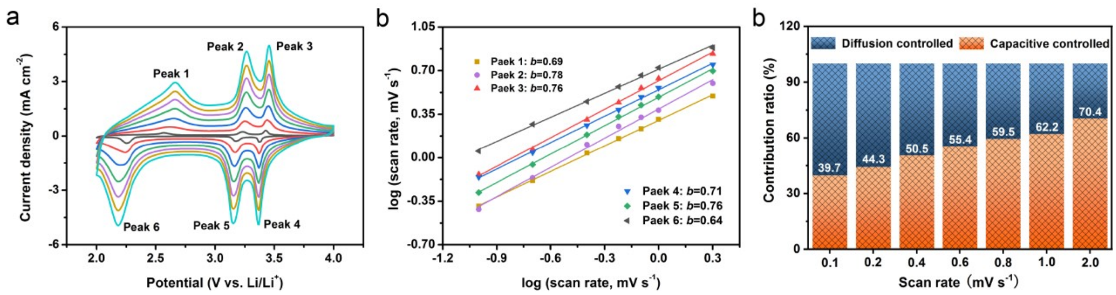

Figure S18. (a) CV curves at different scan rates, (b) log (i) vs. log (v) plots at six peaks in (a), (c) Surface capacitive contributions of α-V_2O_5 NS electrode at various scan rates.

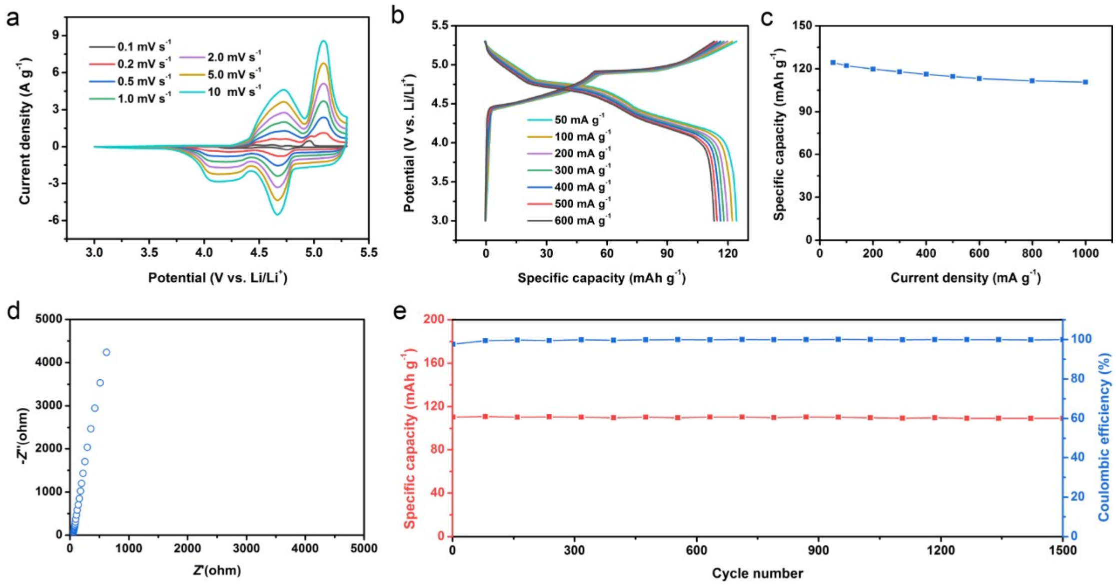

Figure S19. Electrochemical performance of the graphite cathode tested in half cell. (a) CV curves collected at various scan rates, (b) GCD curves measured at different current density, (c) Specific capacity as a function of current density, (d) Nyquist plots, and (e) cycling performance at 1000 mA g^{-1}.

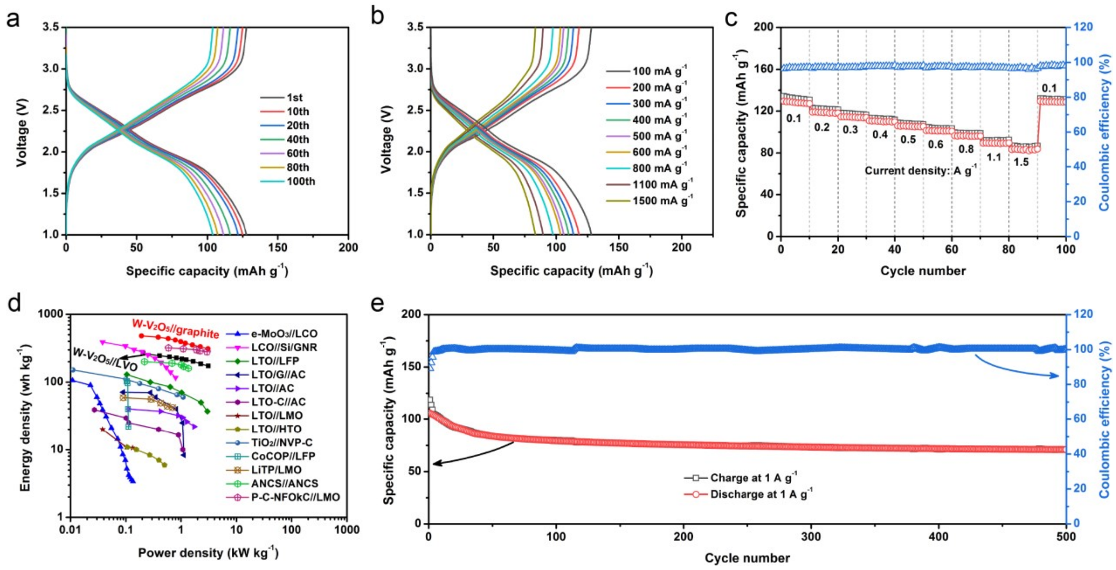

Figure S20. Electrochemical performance of W-V_2O_5//Li_3VO_4 device. (a) GCD curves of various cycle number at 100 mA g^{-1}, (b) GCD curves measured at different current density, (c) rate capability and Coulombic efficiency. (d) Ragone plots of W-V_2O_5//Li_3VO_4 device in comparison with the recently reported lithium ion batteries devices, and (e) cycle durability at 1 A g^{-1}.

References

1. C. Peng, F. Xiao, J. Yang, Z.h. Li, G.t. Lei, Q.z. Xiao, Y.h. Ding and Z.L. Hu, Carbon-encapsulated Mn-doped V_2O_5 nanorods with long span life for high-power rechargeable lithium batteries. *Electrochim. Acta*, 2016, **192**, 216-226.
2. B. Yan, X.F. Li, Z.M. Bai, Y. Zhao, L. Dong, X.S. Song, D.J. Li, C. Langford and X.L. Sun, Crumpled reduced graphene oxide conformally encapsulated hollow V_2O_5 nano/microsphere achieving brilliant lithium storage performance. *Nano*

Energy, 2016, **24**, 32-44.

3. Q.F. Li, D. Chen, H.T. Tan, X.H. Zhang, X.H. Rui and Y. Yu, 3D porous V_2O_5 architectures for high-rate lithium storage. *J. Energy Chem.*, 2020, **40**, 15-21.
4. Y.J. Zhu, M. Yang, Q.Y. Huang, D.R. Wang, R.B. Yu, J.Y. Wang, Z.J. Zheng and D. Wang, V_2O_5 textile cathodes with high capacity and stability for flexible lithium‐ion batteries. *Adv. Mater.*, 2020, **32**, 1906205.
5. J. Zeng, J.D. Huang, J. Liu, T. Xie, C.Q. Peng, Y.K. Lu, P.J. Lu, R.Z. Zhang and J. Min, Self-assembly of single layer V_2O_5 nanoribbon/graphene heterostructures as ultrahigh-performance cathode materials for lithium-ion batteries. *Carbon*, 2019, **154**, 24-32.
6. Q. Li, Y.F. Chen, J.R. He, F. Fu, F. Qi, J. Lin and W.L. Zhang, Carbon Nanotube Modified V_2O_5 Porous Microspheres as Cathodes for High-Performance Lithium-Ion Batteries. *Energy Technol.*, 2017, **5**, 665-669.
7. D.B. Kong, X.L. Li, Y.B. Zhang, X. Hai, B. Wang, X.Y. Qiu, Q. Song, Q.H. Yang and L.J. Zhi, Encapsulating V_2O_5 into carbon nanotubes enables the synthesis of flexible high-performance lithium ion batteries. *Energy Environ Sci.*, 2016, **9**, 906-911.
8. J.M. Son, S. Oh, S.H. Bae, S. Nam and I.K. Oh, A Pair of $NiCo_2O_4$ and V_2O_5 Nanowires Directly Grown on Carbon Fabric for Highly Bendable Lithium‐Ion Batteries. *Adv. Energy Mater.*, 2019, **9**, 1900477.
9. Y.Z. Zheng, H.Y. Ding, E. Uchaker, X. Tao, J.F. Chen, Q.F. Zhang and G.Z. Cao, Nickel-mediated polyol synthesis of hierarchical V_2O_5 hollow microspheres with

enhanced lithium storage properties. *J. Mater. Chem. A*, 2015, **3**, 1979-1985.

10. B. Sun, K. Huang, X. Qi, X.L. Wei and J.X. Zhong, Rational Construction of a Functionalized V_2O_5 Nanosphere/MWCNT Layer-by-Layer Nanoarchitecture as Cathode for Enhanced Performance of Lithium-Ion Batteries. *Adv. Funct. Mater.*, 2015, **25**, 5633-5639.
11. A.Q. Pan, H.B. Wu, L. Yu and X.W. Lou, Template‐free synthesis of VO_2 hollow microspheres with various interiors and their conversion into V_2O_5 for lithium-ion batteries. *Angew. Chem.*, 2013, **125**, 2282-2286.
12. Y.F. Dou, X. Liang, G.H. Gao and G.M. Wu, Template-free synthesis of porous V_2O_5 yolk-shell microspheres as cathode materials for lithium ion batteries. *J. Alloy. Compd.*, 2018, **735**, 109-116.
13. H. Tan, X.Z. Yu, K. Huang, J.X. Zhong and B.A. Lu, Large-scale carambola-like V_2O_5 nanoflowers arrays on microporous reed carbon as improved electrochemical performances lithium-ion batteries cathode. *J. Energy Chem.*, 2020, **51**, 388-395.
14. M.H. Chen, X.H. Xia, J.F. Yuan, J.H. Yin and Q.G. Chen, Free-standing three-dimensional continuous multilayer V_2O_5 hollow sphere arrays as high-performance cathode for lithium batteries. *J. Power Sources*, 2015, **288**, 145-149.
15. X.H. Rui, Y.X. Tang, O.I. Malyi, A. Gusak, Y.Y. Zhang, Z.Q. Niu, H.T. Tan, C. Persson, X.D. Chen, Z. Chen and Q.Y. Yan, Ambient dissolution–recrystallization towards large-scale preparation of V_2O_5 nanobelts for high-energy battery applications. *Nano Energy*, 2016, **22**, 583-593.

16. S. Wang, P.Y. Zhang, H. Tan, X.Y. Fan and K. Huang, V_2O_5 nanosheets anchored on graphitized carbon nanofibers network for free-standing cathode on performance-improved lithium ion batteries. *J. Power Sources,* 2019, **419**, 106-111.

17. G.Z. Li, Y.C. Qiu, Y. Hou, H.F. Li, L.S. Zhou, H. Deng and Y.G. Zhang, Synthesis of V_2O_5 hierarchical structures for long cycle-life lithium-ion storage. *J. Mater. Chem. A*, 2015, **3**, 1103-1109.

18. N. Xu, J.Q. Liang, T. Qian, T.Z. Yang and C.L. Yan, Half-cell and full-cell applications of horizontally aligned reduced oxide graphene/V_2O_5 sheets as cathodes for high stability lithium-ion batteries. *RSC Adv.*, 2016, **6**, 98581-98587.

19. X. Peng, X.M. Zhang, L. Wang, L.S. Hu, S.H.S. Cheng, C. Huang, B. Gao, F. Ma, K.F. Huo and P.K. Chu, Hydrogenated V_2O_5 nanosheets for superior lithium storage properties. *Adv. Funct. Mater.*, 2016, **26**, 784-791.

20. M.M. Rahman, A.Z. Sadek, I. Sultana, M. Srikanth, X.J. Dai, M.R. Field, D.G. McCulloch, S.B. Ponraj and Y. Chen, Self-assembled V_2O_5 interconnected microspheres produced in a fish-water electrolyte medium as a high-performance lithium-ion-battery cathode. *Nano Res.*, 2015, **8**, 3591-3603.

21. L.Q. Mai, Q.Y. An, Q.L. Wei, J.Y. Fei, P.F. Zhang, X. Xu, Y.L. Zhao, M.Y. Yan, W. Wen and L. Xu, Nanoflakes-Assembled Three-Dimensional Hollow-Porous V_2O_5 as Lithium Storage Cathodes with High-Rate Capacity. *Small*, 2014, **10**, 3032-3037.

22. J.F. Huang, X.N. Qiao, Z.W. Xu, L.Y. Cao, H.B. Ouyang, J.Y. Li and R.Y. Wang,

V_2O_5 self-assembled nanosheets as high stable cathodes for Lithium-ion batteries. *Electrochim. Acta*, 2016, **191**, 158-164.

23. S.K. Park, P. Nakhanivej, J.S. Yeon, K.H. Shin, W.M. Dose, M. De Volder, J.B. Lee, H.J. Kim and H.S. Park, Electrochemical and structural evolution of structured V_2O_5 microspheres during Li-ion intercalation. *J. Energy Chemistry*, 2021, **55**, 108-113.
24. X.T. Gao, X.D. Zhu, S.R. Le, D.J. Yan, C.Y. Qu, Y.J. Feng, K.N. Sun and Y.T. Liu, Boosting High-Rate Lithium Storage of V2O5 Nanowires by Self-Assembly on N-Doped Graphene Nanosheets. *ChemElectroChem*, 2016, **3**, 1730-1736.
25. N.T. Wu, W.Z. Du, G.L. Liu, Z. Zhou, H.R. Fu, Q.Q. Tang, X.M. Liu and Y.B. He, Synthesis of hierarchical sisal-like V_2O_5 with exposed stable {001} facets as long life cathode materials for advanced lithium-ion batteries. *ACS Appl. Mater. Interfaces*, 2017, **9**, 43681-43687.
26. Y.L. Shan, L. Xu, Y.J. Hu, H. Jiang and C.Z. Li, Internal-diffusion controlled synthesis of V_2O_5 hollow microspheres for superior lithium-ion full batteries. *Chem. Eng. Sci.*, 2019, **200**, 38-45.
27. K. Ma, X. Liu, Q.L. Cheng, P. Saha, H. Jiang and C.Z. Li, Flexible textile electrode with high areal capacity from hierarchical V_2O_5 nanosheet arrays. *J. Power Sources*, 2017, **357**, 71-76.
28. J.H. Lee, J.M. Kim, J.H. Kim, Y.R. Jang, J.A. Kim, S.H. Yeon and S.Y. Lee, Toward Ultrahigh‐Capacity V_2O_5 Lithium-Ion Battery Cathodes via One-Pot Synthetic Route from Precursors to Electrode Sheets. *Adv. Mater. Interfaces*, 2016,

3, 1600173.